**Climate
of the Past**

Open Access

EGU

Supplement of

Warm mid-Pliocene conditions without high climate sensitivity: the CCSM4-Utrecht (CESM 1.0.5) contribution to the PlioMIP2

Michiel L. J. Baatsen et al.

Correspondence to: Michiel L. J. Baatsen (m.l.j.baatsen@uu.nl)

Table S1. Implemented fraction of CLM4 plant functional types (PFTs; see below) for each of the given PRISM4 megabiomes.

Megabiome	#	0	1	2	3	4	5	6	7	8	9	10	11	12	13	14
Tropical forest	1					0.75		0.25								
Warm-temperate forest	2		0.34				0.33		0.33							
Savannah and dry woodland	3		0.125				0.15	0.125	0.125		0.05					0.425
Grassland and dry shrubland	4						0.1	0.25			0.15					0.5
Desert	5	1														
Temperate Forest	6		0.3	0.2			0.2		0.25	0.05						
Boreal Forest	7			0.4	0.425					0.05			0.125			
Tundra	8												0.66	0.34		
Dry tundra	9													1		
Ice	28	1														

0. Bare; Not vegetated;
1. M NET; Needleleaf evergreen temperate tree;
2. B NET; Needleleaf evergreen boreal tree;
3. B NDT; Needleleaf deciduous boreal tree;
4. T BET; Broadleaf evergreen tropical tree;
5. M BET; Broadleaf evergreen temperate tree;
6. T BDT; Broadleaf deciduous tropical tree;
7. M BDT; Broadleaf deciduous temperate tree;

8. B BDT; Broadleaf deciduous boreal tree;
9. M BES; Broadleaf evergreen shrub;
10. T BDS; Broadleaf deciduous tropical shrub;
11. B BDS; Broadleaf deciduous boreal shrub;
12. C3 Arc; C3 arctic grass;
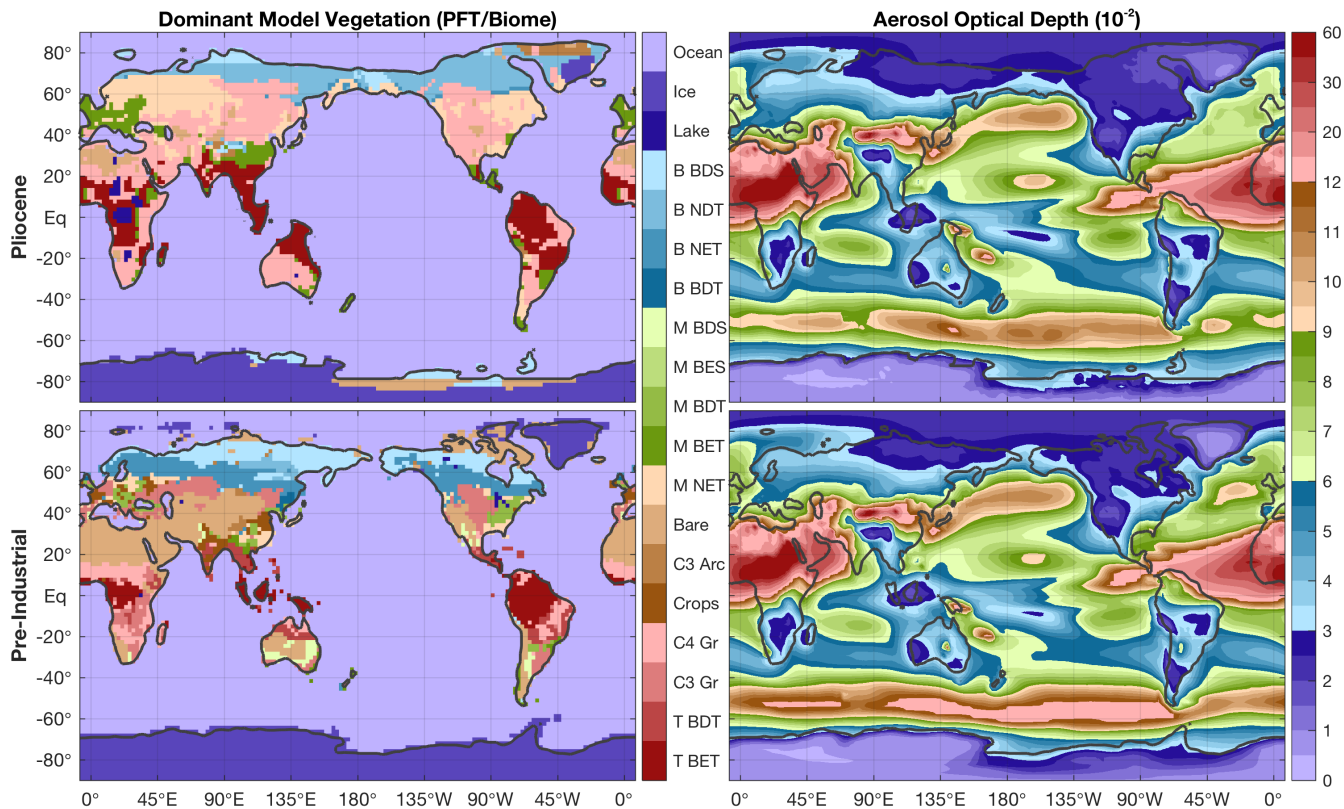13. C3 Gr; C3 non-arctic grass;
14. C4 Gr; C4 grass.

Figure S1. Pliocene (upper panels) and pre-industrial (lower panels) surface properties (left) and annual mean aerosol optical depth(right) in our model simulations. Vegetation is characterised by its dominant plant functional type, of which the used acronyms are given in Table S1.
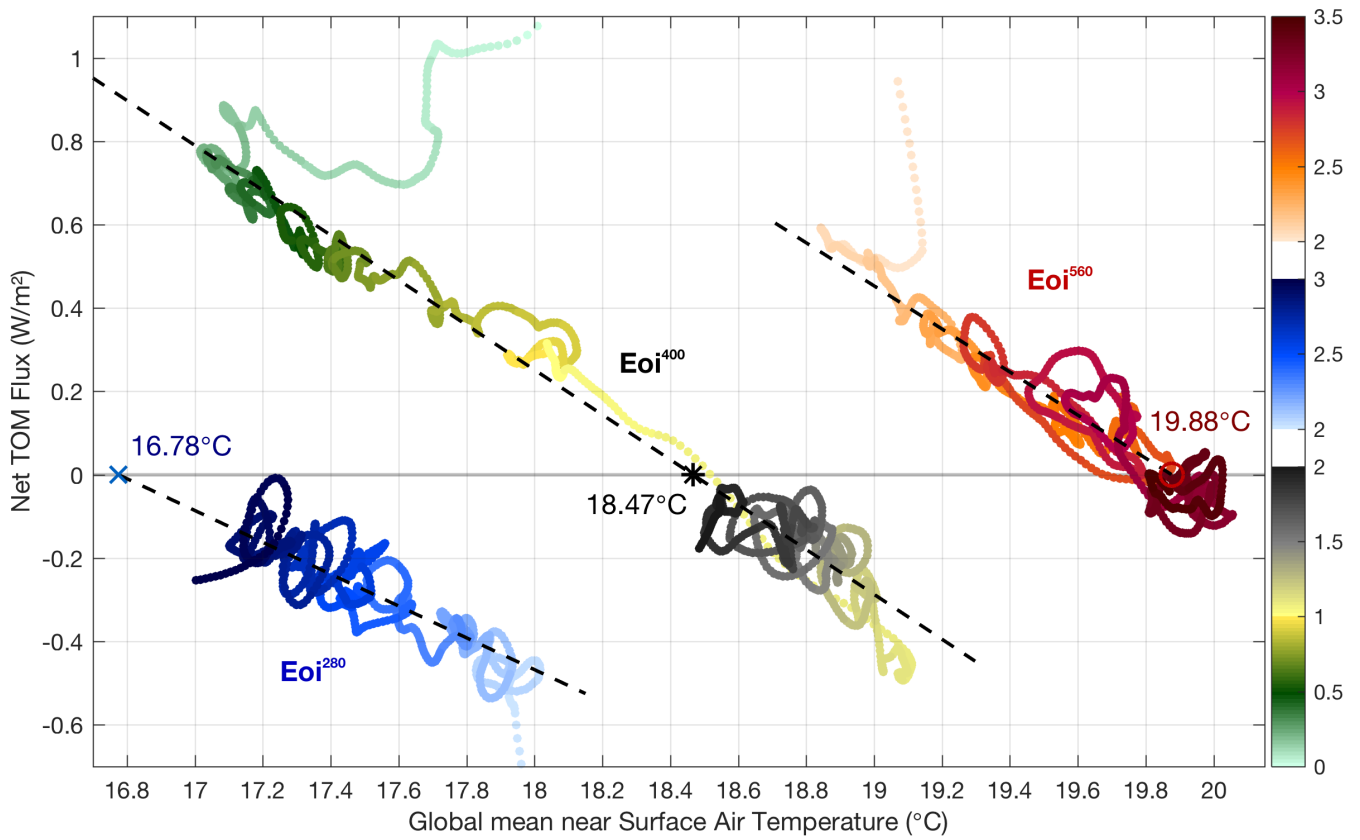
Figure S2. Full equilibration of our three Pliocene simulations: Eoi[280] (blue), Eoi[400] (green-yellow), and Eoi[560] (red), using the globally averaged annual mean near surface temperature and net top of model radiative flux. A 30-year smoothing average was applied to both time series, which are colour coded as a function of the model year (in kyr).
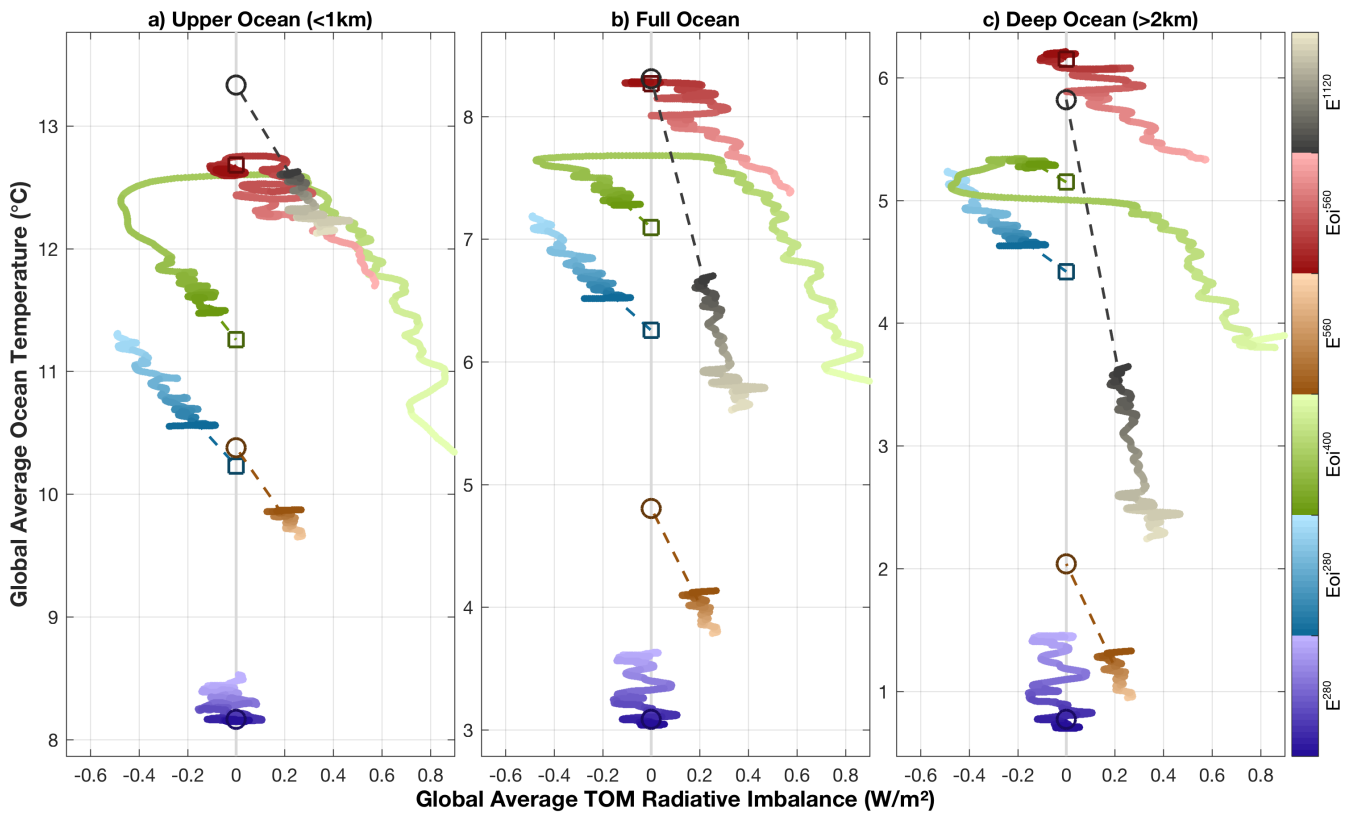
Figure S3. Full equilibration of our three standard pre-industrial (E^{280}, E^{560}, and E^{1120}) and Pliocene (Eoi^{280}, Eoi^{400}, and Eoi^{560}) cases, colour coded for the length of each simulation. As a function of annual mean, globally averaged top of model net radiative flux, we show **a)** upper (<1km), **b)** full depth, and **c)** deep (>2km) ocean average temperature. A 50-year smoothing average was applied to the time series, along with an extrapolation towards net radiative balance using a linear regression over the last 750 model years of each simulation.
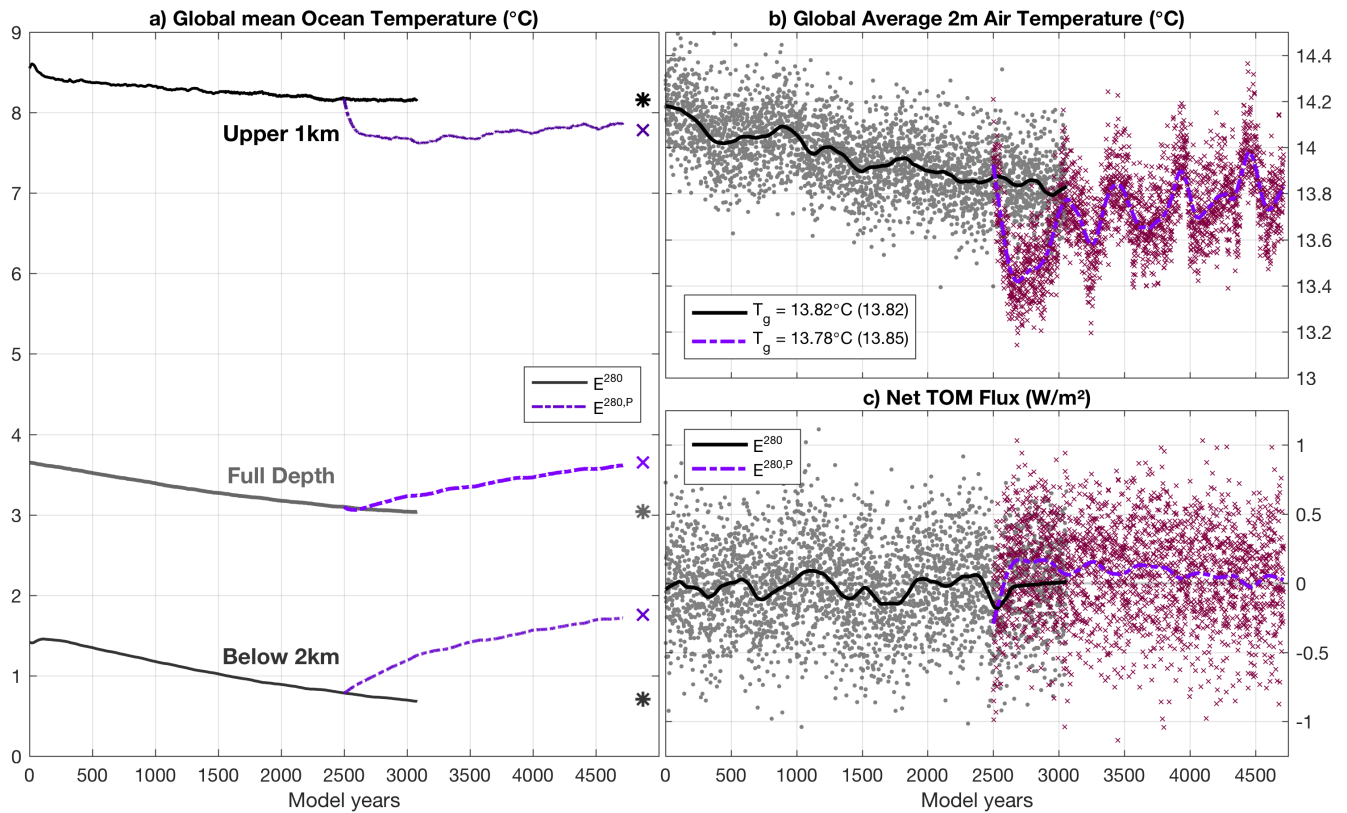
Figure S4. Time series of globally averaged temperatures for the entire length of our 2 main pre-industrial reference simulations: E^{280} (black), and $E^{280,P}$ (purple). Shown are the **a)** upper (<1km; dark), deep (>2km; medium), and full depth (light) ocean temperature, **b)** near surface air temperature, and **c)** globally averaged top of model (TOM) net radiative flux. Thick lines in b,c show the corresponding time series after applying a 200-year smoothing mask. The estimated equilibrium temperatures are indicated at the end in a,b, using large markers and the same colour convention. The globally averaged, mean temperature (T_g) over the last 100 years is added in the legend of b (bracketed values for the estimated equilibrium).
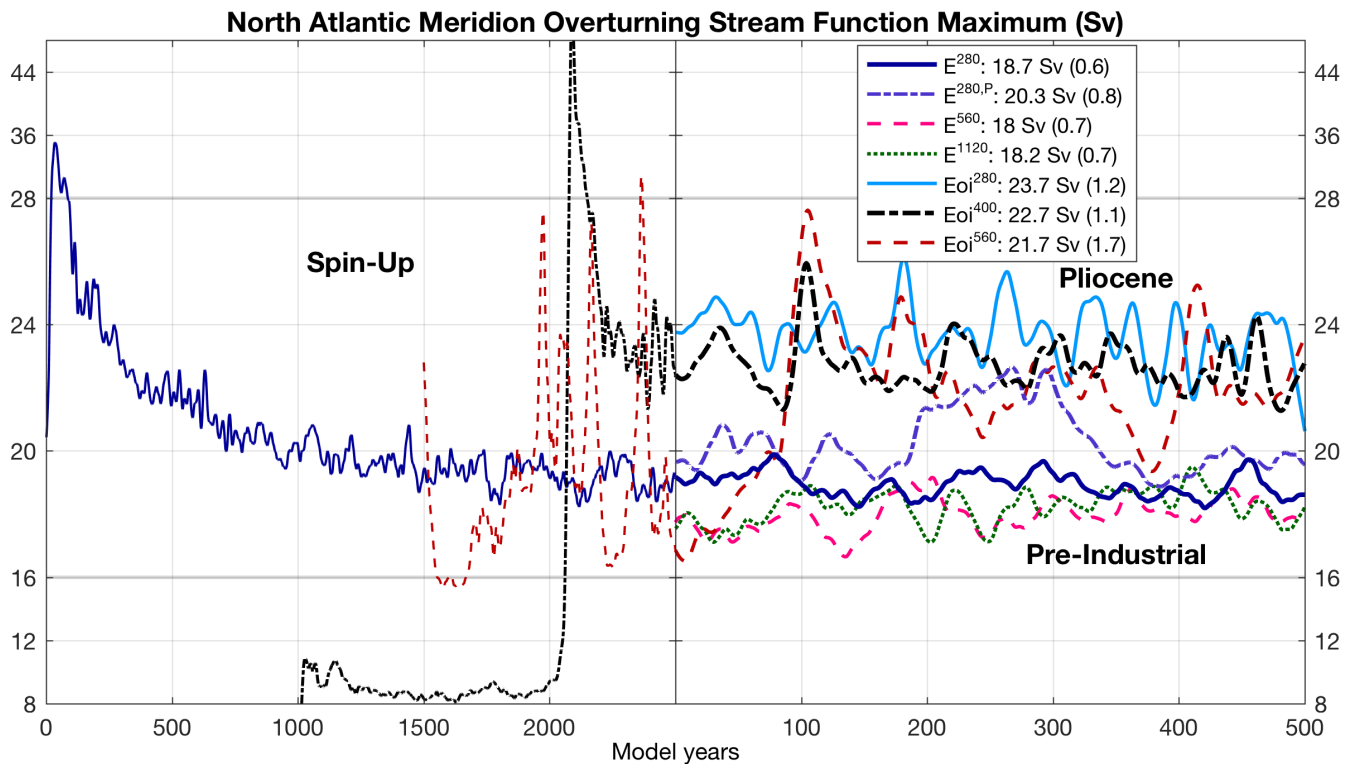
Figure S5. Time series of the annual mean AMOC strength (i.e. stream function maximum below 1km) for all 7 simulations, using a 20-year smoothing window. The last 500 years are aligned and shown in detail, with the full spinup of the E^{280}, Eoi^{400}, and Eoi^{560} added on the left (note the different time scale). The average over the last 500 years is given in the legend for each case, with the corresponding standard deviation shown in brackets. Standard deviation is applied to the de-trended AMOC time series using a 250-year smoothing average.
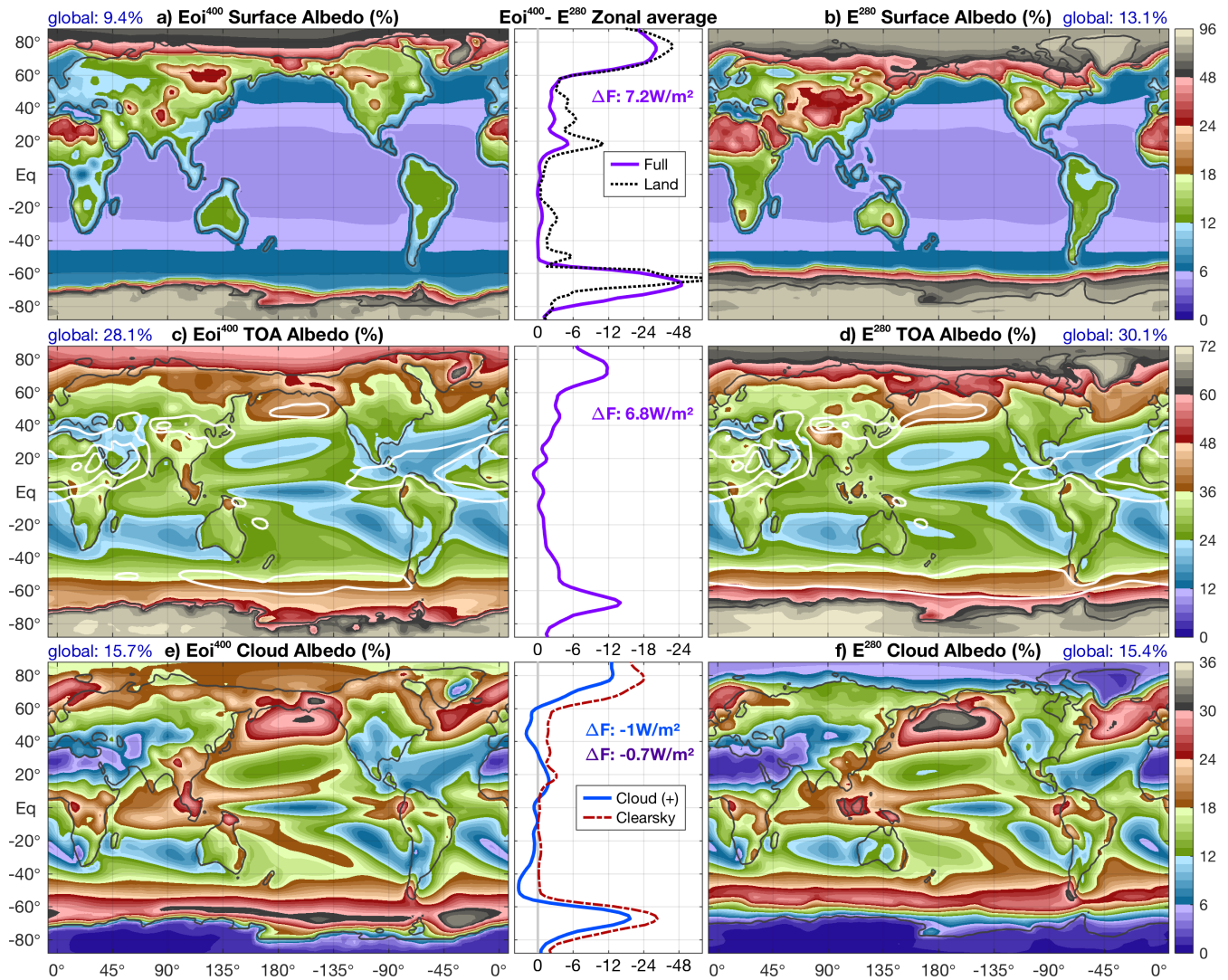
Figure S6. Annual mean albedo in the E^{280} (left) and Eoi^{400} (right) simulation, using the colour scales shown to the right. Shown from top to bottom are surface, top of atmosphere (TOA), and cloud albedo, with white contours in the TOA figures indicating aerosol optical depth at 0.1, 0.2, and 0.4 (see also Figure S1). The corresponding zonal average Eoi^{400}- E^{280} differences are given in the middle panels (note the negative scale; positive for cloud albedo). The resulting global average radiative forcing from each component is given, with the cloud forcing subdivided into shortwave-only (blue) and total (purple).
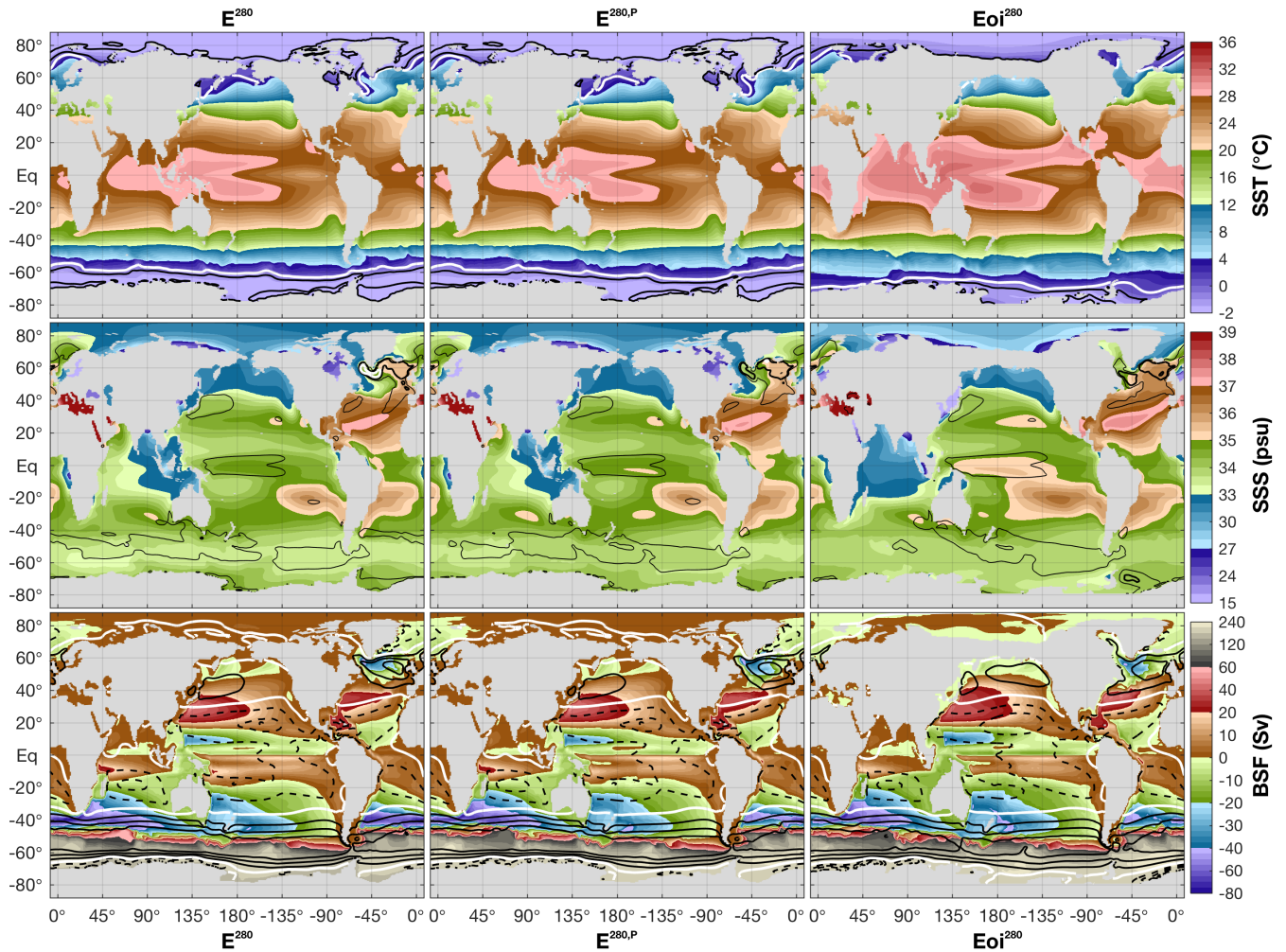
Figure S7. Annual mean oceanic fields from the (left to right) E^{280}, $E^{280,P}$, and Eoi^{280} cases. **Top**: sea surface temperature temperature (shading) and sea ice fraction (contours; white: 0.15, black: 0.5 and 0.9). **Middle**: Sea surface salinity (shading) and mixed layer depth (contours; black: 100m, thick black: 250m, thick white: 500m). **Bottom**: Barotropic stream function (BSF; shading) and zonal wind stress (contours every $5 \cdot 10^{-2}$Pa, dashed: <0, thick white line at 0hPa).
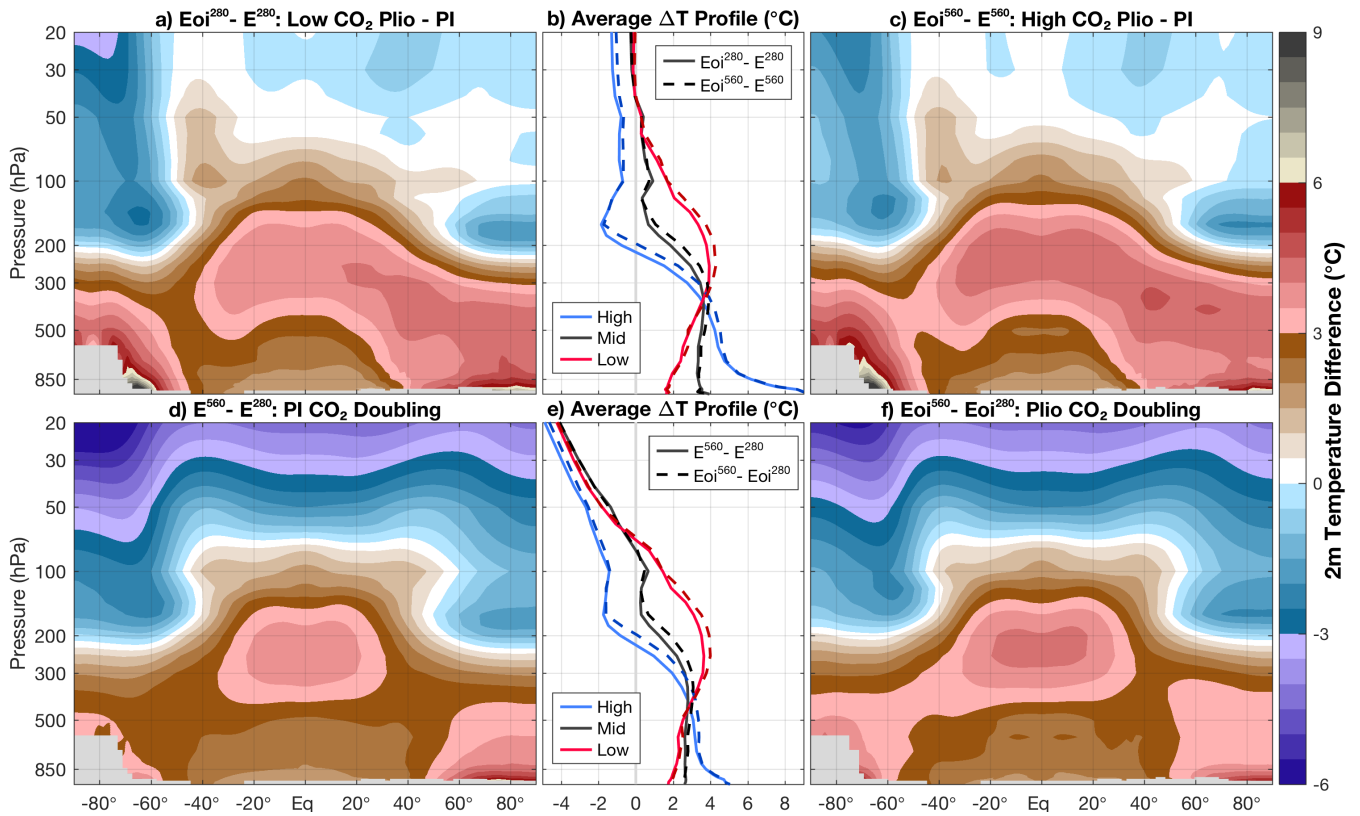
Figure S8. Annual mean, zonally averaged air temperature difference as a function of pressure, between our four *sensitivity* simulations; **a)** Eoi^{280} - E^{280}, **c)** Eoi^{560} - E^{560}, **d)** E^{560} - E^{280}, and **f)** Eoi^{560} - Eoi^{280}. **b)** Average vertical temperature difference profile of Eoi^{280} - E^{280} (solid) and Eoi^{560} - E^{560} (dashed) for high (>60°; blue), middle (30–60°; black), and low (<30°; red) latitudes. **e)** As in b, but for E^{560} - E^{280} (solid) and Eoi^{560} - Eoi^{280} (dashed).

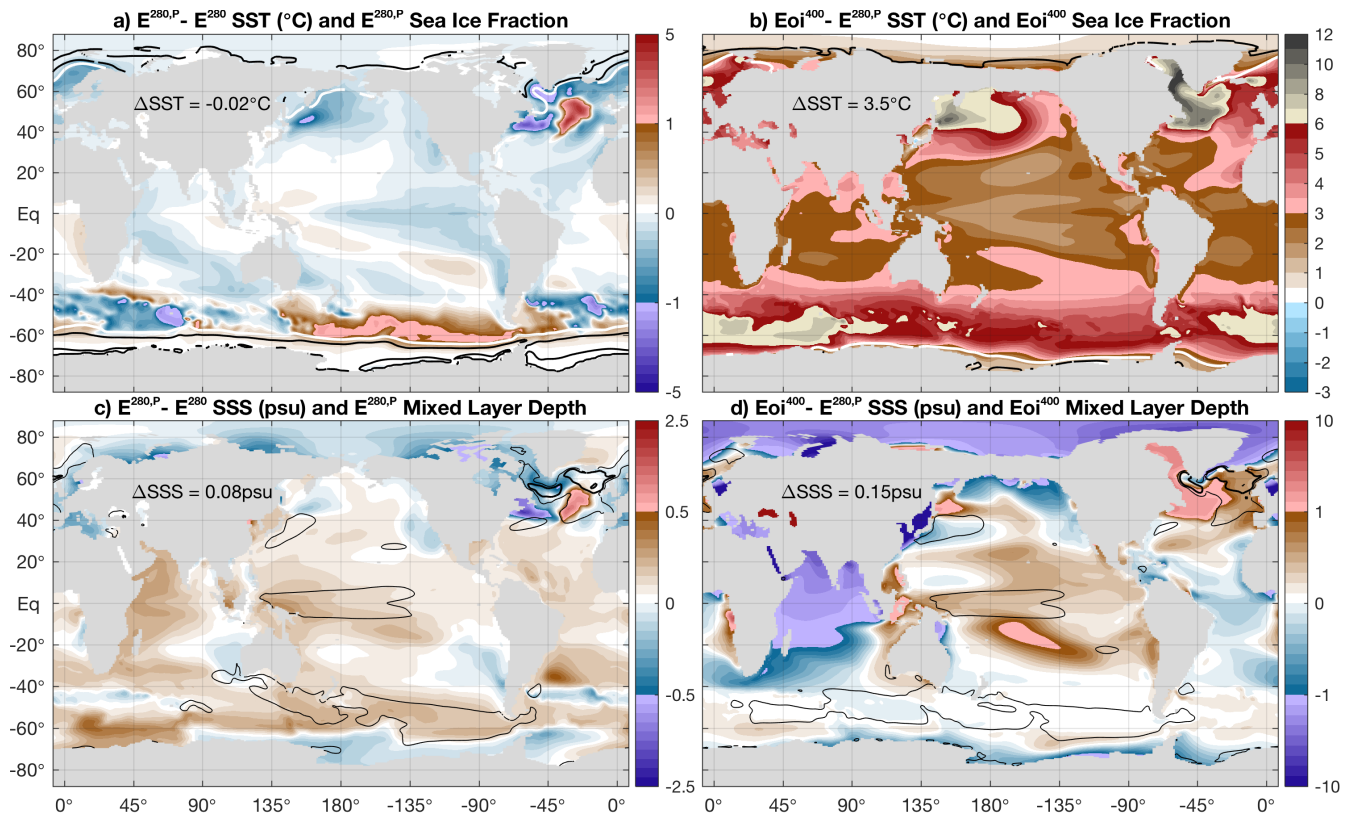**Figure S9.** Annual mean SST difference between **a)** $E^{280,P}$- E^{280}, and **b)** Eoi^{400}- $E^{280,P}$. The global average difference (ΔSST) is given, contours show $E^{280,P}$ (a) and Eoi^{400} (b) annual mean sea ice fraction (white: 15%, black: 50% and 90%). **c,d)** As in a,b but for sea surface salinity difference (shading) and mixed layer depth (contours; black: 100m, thick black: 250m, and white: 500m).
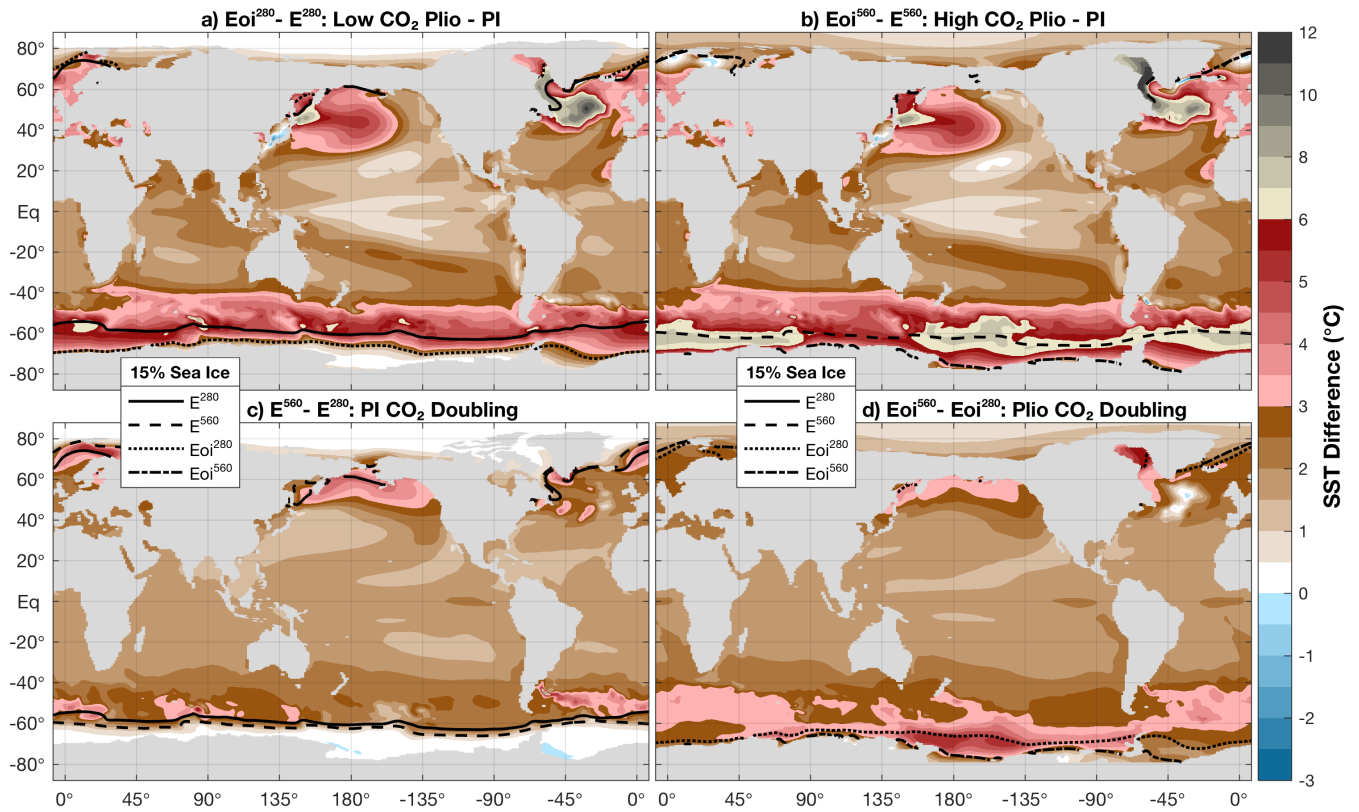
Figure S10. Annual mean sea surface temperature (SST) difference between our four *sensitivity* simulations; **a)** Eoi[280]- E[280], **b)** Eoi[560]- E[560], **c)** E[560]- E[280], and **d)** Eoi[560]- Eoi[280]. Contours showing the annual mean sea ice edge (i.e. 0.15 ice fraction) in black; solid: E[280], dashed: E[560], dotted: Eoi[280], and dash-dotted: Eoi[560] (2 shown per panel).
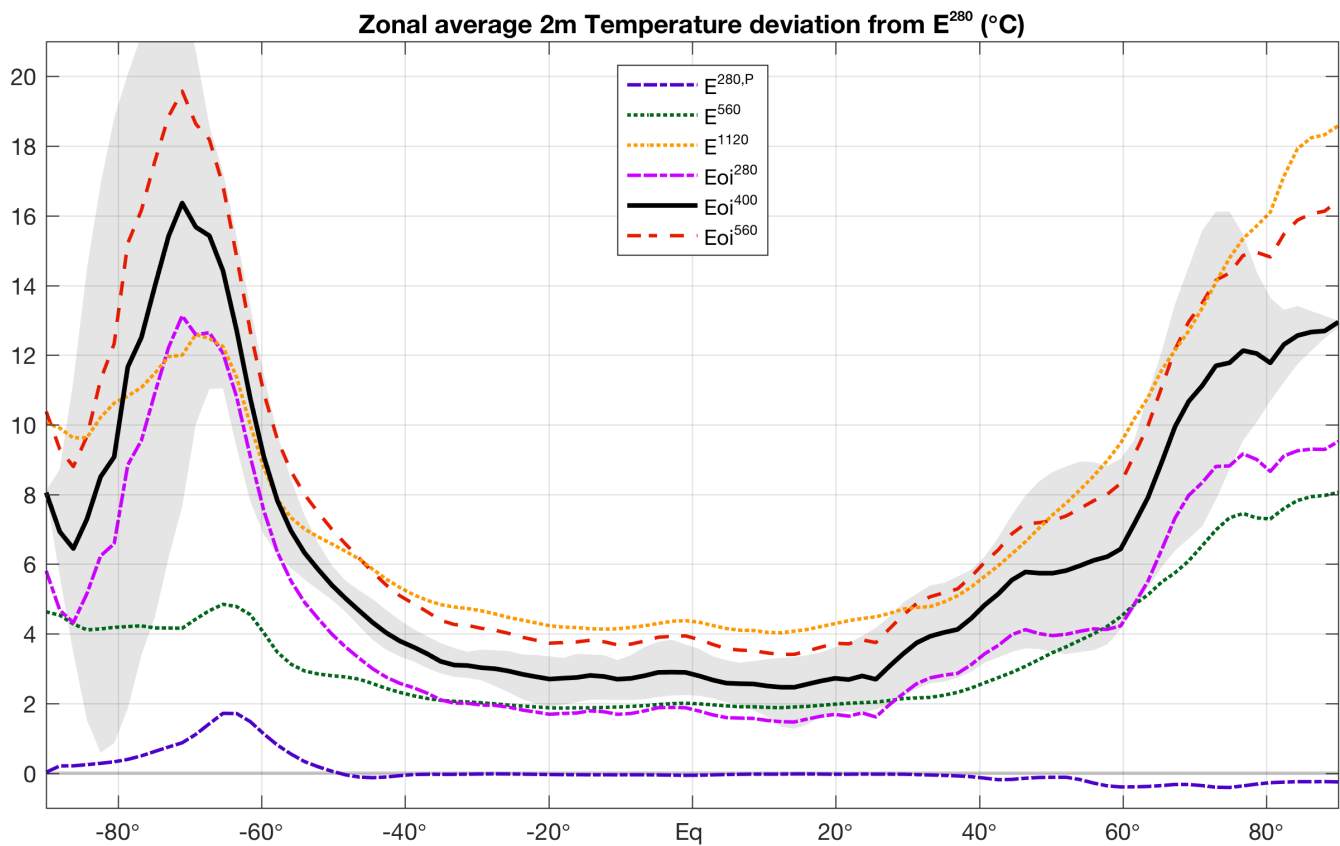
Figure S11. Zonally averaged near surface air temperature difference of each model case from the E^{280} pre-industrial reference, with the zonal variation (10 and 90 percentiles) of the Eoi^{400}- E^{280} indicated in gray shading.
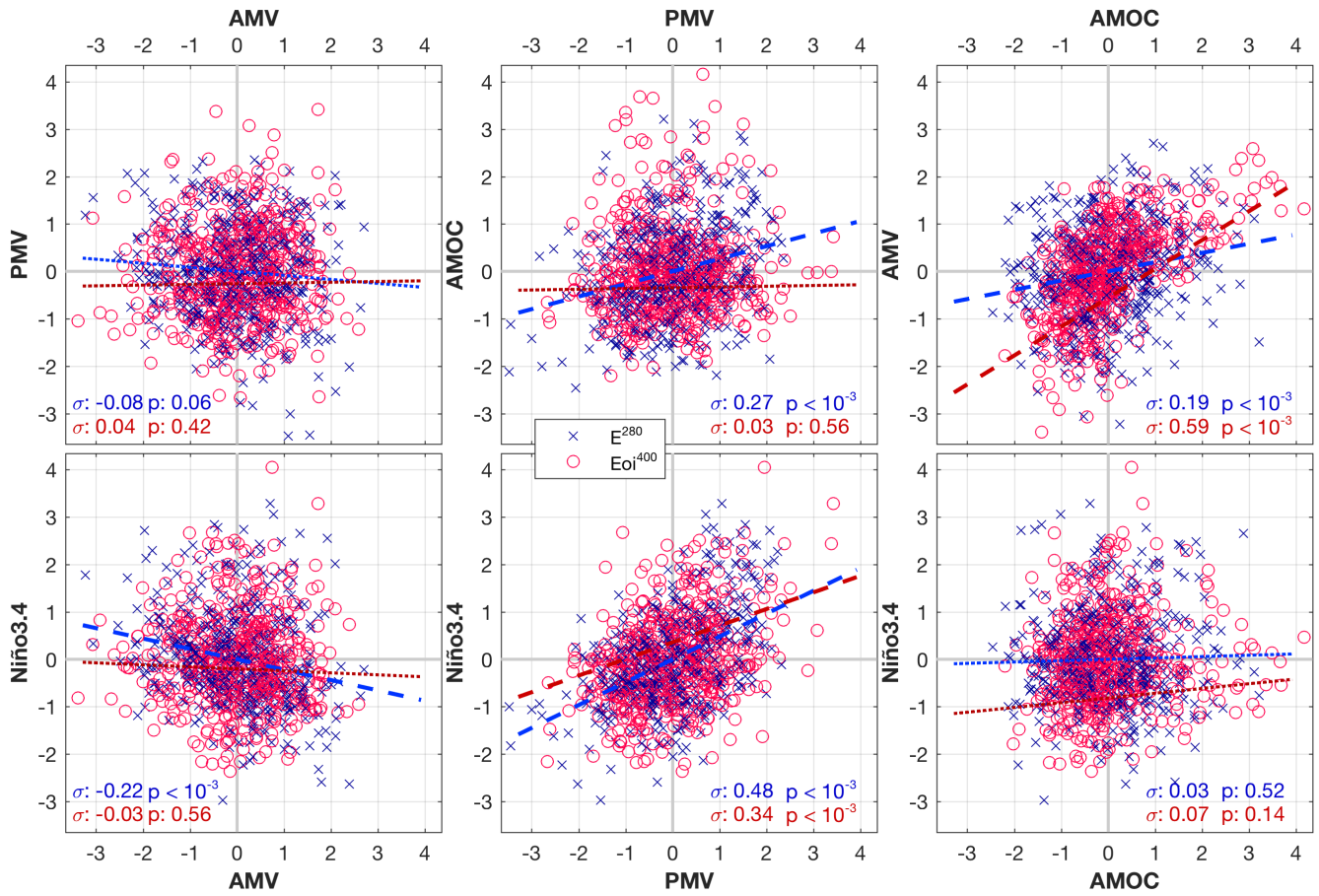
Figure S12. Scatter plots of annual mean AMV, PMV, AMOC, and Niño 3.4 indices of the E^{280} (blue crosses) and Eoi^{400} (red cricles) using 500 years of SST data. Cross correlations between the different indices are given along with their p-value. Coloured lines in corresponding colours for each simulation show a linear regression, with thick dashed lines used for statistically significant correlations (i.e. p-value <0.05).